JOURNAL OF MATERIALS SCIENCE 32 (1997) 5205–5213

Electrochemical Al_2O_3–Cr_2O_3 alloy coatings on non-oxide ceramic substrates

I. ZHITOMIRSKY, R. CHAIM*, L. GAL-OR
*Israel Institute of Metals, and *Department of Materials Engineering, Technion, Israel Institute of Technology, Haifa 32000 Israel*

H. BESTGEN
Hoechst AG, ZF-Methodische Projekts, 65926 Frankfurt/Main, Germany

Aqueous solutions of $xAl(NO_3)_3 + (1-x)Cr(NO_3)_3$ were used for electrodeposition of ceramic Al_2O_3–Cr_2O_3 alloy coatings on TiC, TiB_2 and SiC substrates. Cell voltage and deposit weight were studied as function of deposition duration, current density and electrolyte composition. It was shown that the electrochemical parameters permit simple control of the deposition process. Optimal current densities and deposition durations were determined to obtain maximal deposit weights for different solutions and substrates. Deposits with thicknesses up to 10 μm were formed. The green deposits revealed a crystalline nature for compositions of $x < 0.3$, and an amorphous nature for $x \geqslant 0.3$, independent of the substrate material. Voltage–electrolyte composition dependencies exhibited an ubiquitous minimum at $x \approx 0.3$ to 0.4 independent of substrate type and deposition duration. These minima were attributed to the change in the electrical resistance of the deposit with composition and degree of crystallinity.

1. Introduction

Recently, a great deal of interest has arisen in the field of electrodeposition of ceramic films and coatings [1–6]. Intensive research has been conducted on electrodeposition of different ceramic coatings, including monolithic oxides [1–4], as well as oxide compounds [5–10]. Electrodeposition was also applied in order to form nanostructured ceramics as well as nanomodulated structures [11, 12]. In the cathodic electrodeposition mode, metal ions are hydrolysed by electrogenerated base to form oxide/hydroxide films on the cathodic substrate. However, in all these investigations, metallic or semiconducting substrates were used as substrate-cathodes. Recently, the feasibility of electrodeposition of oxides on non-oxide ceramic substrates has been demonstrated, where aluminium, chromium and zirconium oxide coatings were applied to TiC, TiB_2 and SiC substrates [13–15]. Non-oxide ceramics are very attractive materials for high-temperature applications owing to their high-temperature strength. Nevertheless, they are often chemically unstable at high temperatures, especially when exposed to oxidizing atmospheres. Although some of the non-oxide ceramics form a native protecting oxide scale (i.e. SiO_2 on SiC) under certain thermodynamic conditions, application of non-native oxide coatings may improve the oxidation resistance of the non-oxide ceramics. Moreover, application of oxide alloys as well as composite oxide coatings with desirable properties may be advantageous. Thus problems associated with thermal expansion mismatch between the coating and the substrate materials may be controlled by variation of coating composition.

High electrical resistance is a major limiting factor in the electrodeposition of oxide coatings with appropriate thicknesses needed for efficient oxidation protection. Owing to the significant difference in the electrical resistance of alumina and chromia [16], alloys of these oxides offer the advantage of providing a desired level of coating resistivity. Al_2O_3–Cr_2O_3 alloys also exhibit increased hardness relative to monolithic alumina [17, 18]. Nevertheless, the physical compatibility of the oxide components, as well as their chemical affinities to the substrate material, should also be considered for controlling coating properties and performance.

The present paper reports the results of the electrochemical codeposition of alumina and chromia on TiC, TiB_2 and SiC substrates. Factors controlling the deposit characteristics were determined and the formation mechanism of the oxide coatings via the electrodeposition process was addressed.

2. Experimental procedure

Commercially pure $Al(NO_3)_3 \cdot 9H_2O$ and $Cr(NO_3)_3 \cdot 9H_2O$ were used as precursor materials. Aqueous solutions of $xAl(NO_3)_3 + (1-x)Cr(NO_3)_3$ ($x = 0.1$–0.9 in steps of 0.1) of a total concentration of 0.1 M were prepared. Ethyl alcohol (ethanol) was added as a wetting agent in the proportion of deionized water to ethanol of 2:1. The conductivity of the solutions was

0022–2461 © 1997 Chapman & Hall

measured using a conductivity meter (El-Hamma Instruments, model TH-2400).

TiC, TiB_2 and SiC bars of $3\,mm \times 3\,mm \times 50\,mm$ were used as substrates; their electrical resistivities were measured to be 5×10^{-5}, 2×10^{-5} and $7\,\Omega\,cm$, respectively. Prior to electrodeposition, the substrates were mechanically polished with 600 grit SiC abrasive paper, washed with distilled water, rinsed with ethanol in an ultrasonic bath and dried in air.

The electrochemical cell included the cathodic substrate centred between two parallel platinum counter-electrodes. Electrodeposition was performed by use of a power supply (Lambda, model LLS 7120). Cell voltage and current were measured with amper-volt-ohm-meters. Experiments were performed at 10 °C within a cooling bath (Frika, model KT 06-43). Cathodic deposits were obtained over a 20 mm length of the bars, at constant current densities (c.d.) ranging from 5–40 mA cm^{-2}. Deposition durations were up to 40 min. The deposits were dried in air at room temperature and characterized using a scanning electron microscope (Jeol, model JSM-840) equipped with an X-ray energy dispersive spectroscopy (EDS). The phase content of the deposits was determined with an X-ray diffractometer (Philips, model PW-1820) operated at 40 kV and 40 mA using monochromatized CuK_α radiation and a scanning speed of 0.4 ° min. The deposit weight was determined by weighing the specimens before and after deposition, with an accuracy of $\pm$ 0.05 mg.

3. Results

3.1. Electrodeposition on TiC substrates

The initial pH and the conductivity of the solutions are important factors which control the deposition process, and were measured prior to electrodeposition. The initial pH increased with x from pH = 2.5 for $x = 0$ to pH = 2.9 for $x = 1.0$. No appreciable changes in the solutions' conductivity (7.2×10^{-3} to $7.6 \times 10^{-3}\,S\,cm^{-1}$) were observed with composition (x = 0–1.0, respectively).

The process has been studied at different current densities and deposition durations. Fig. 1 shows the cell voltage during the deposition process at 5, 20 and 40 mA cm^{-2} for an aluminium-rich solution ($x = 0.9$). At higher current densities, the voltage increased with time to reach a maximum at shorter durations. The voltage reached a maximum after $\sim$ 2 and 6 min for current densities of 40 and 20 mA cm^{-2}, respectively. At a lower current density of 5 mA cm^{-2}, the voltage increase was moderate, and the plateau was reached after a relatively long duration (36 min). In addition, at 40 mA cm^{-2} the voltage continuously decreased after the maximum, to a saturation level.

Fig. 2 shows the deposit weight versus current density for chromium-rich ($x = 0.1$) and aluminium-rich ($x = 0.9$) solutions, at a deposition duration of 5 min. The deposit weight increased with current density to show a maximum. Further increase in c.d. beyond the maximum led to spalling of the deposit and its sedimentation on the bottom of the bath. Although a second increase in deposit weight was observed at 25 mA cm^{-2} in the aluminium-rich solution, the current density of 5 mA cm^{-2} was selected for further experiments. This current density was selected because it allowed a smoother coating morphology with less spallation to be obtained.

Deposit weight versus deposition duration for chromium-rich and aluminium-rich solutions at 5 mA cm^{-2} are shown in Fig. 3. As expected, deposit weight increased continuously with deposition

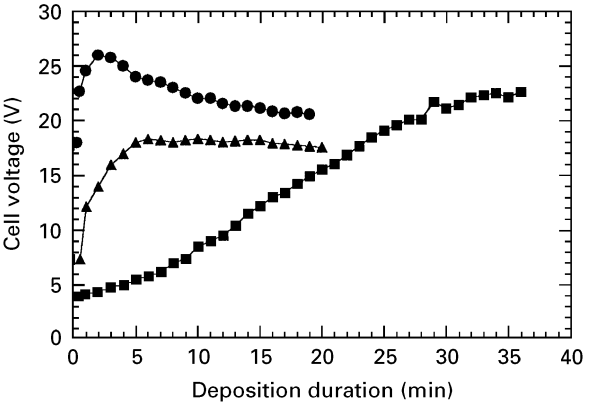

Figure 1 Cell voltage versus deposition duration for 0.1 M aluminium-rich solution ($x = 0.9$) on TiC substrates at current densities of (■) 5, (▲) 20 and (●) 40 mA cm^{-2}.

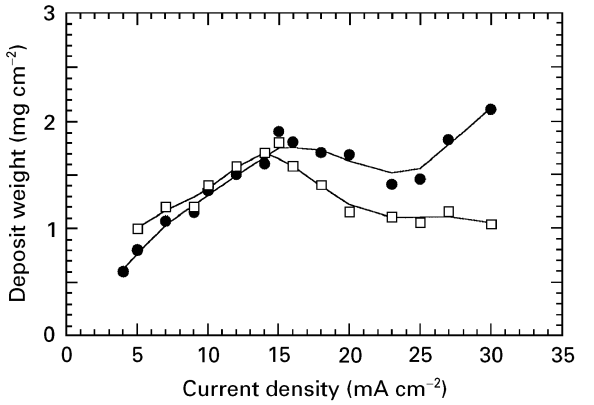

Figure 2 Deposit weight versus current density for TiC substrates in chromium-rich (□, $x = 0.1$) and aluminium-rich (●, $x = 0.9$) solutions; deposition duration 5 min.

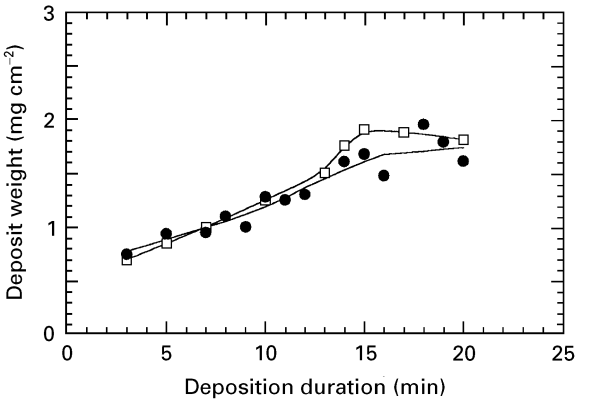

Figure 3 Deposit weight versus deposition duration for TiC substrates in chromium-rich (□, $x = 0.1$) and aluminium-rich (●, $x = 0.9$) solutions; c.d. 5 mA cm^{-2}.

duration. However, at durations higher than 15–20 min, the deposit spalling resulted in a decrease of the deposit weight. In order to prevent deposit spallation, the deposition durations were limited to 15 min.

By drawing the deposit weight versus the transferred charge to the cathode, and using the data for constant deposition duration (Fig. 2) and current density (Fig. 3) experiments, one can determine a master curve for deposition conditions, as shown in Fig. 4. Thus, for a given transferred charge, it is possible to estimate the accumulated deposit weight on the cathode, within the domain of continuous coating. This master curve also indicates the value of the transferred charge (~ 4 C) above which the coating may spal either due to high c.d.s (constant duration curve) or long deposition durations (constant c.d.). Increase in c.d. is expected to cause uniform evolution of molecular hydrogen at the cathode surfaces, which in turn breaks up the deposit. Nevertheless, at lower current densities and longer deposition durations, deposit thickening may be a limiting factor for the charge transfer towards the growing oxide front. Thus, any defect within the deposit may act as a rapid passage for the charge transfer. Such regions will be associated with high local current densities which again enable formation of molecular hydrogen and consequent spalling of the deposit, even though with less damage due to their localized nature.

As was shown above, the cell voltage changes during electrodeposition due to the oxy-hydroxide deposit build-up, which basically has a non-conductive character. Fig. 5 shows the cell voltage versus electrolyte composition at constant deposition durations. These curves exhibit the effect of deposit composition on the cell voltage. For a given c.d., the cell voltage was almost similar for all electrolyte compositions at the begining of the electrodeposition process (i.e. 2 min curve in Fig. 5). However, the cell voltage changed in a different manner for each composition during the process. For all the curves, minima were observed for a composition of $x \approx 0.4$. Generally, the voltage increased with deposition duration. However, higher voltages were recorded with time for aluminium-rich solutions ($x \gg 0.4$) rather than for chromium-rich solutions ($x \ll 0.4$).

These differences in the cell voltage may be attributed to different deposition rates of the two oxide constituents from the solution. This point was checked by plotting the deposit weight as a function of electrolyte composition at constant deposition duration (15 min) and current density (5 mA cm^{-2}) as shown in Fig. 6. The deposit weight was found to decrease linearly with increase in x. This may indicate a more efficient deposition of the chromium component of the deposit. Nevertheless, the cell voltage is not influenced by the deposition rate of the two oxide constituents from the solution.

X-ray diffraction (XRD) spectra from the as-dried deposits on TiC substrates are shown in Fig. 7. The XRD spectra for electrolyte compositions between $x = 0.1$ and 0.3 showed well-defined peaks of the crystalline hydrated chromium oxide ($Cr(OH)_3 \cdot 3H_2O$; JCPDS 16-817) in addition to the peaks from the TiC substrate (peaks marked "○"). The relative intensities of the peaks from the deposit decreased with increase in x. For electrolyte compositions above $x = 0.3$ no evidence for crystalline deposits was found. The present XRD results are in good agreement with the previous findings upon which pure components have shown either an amorphous nature (aluminium oxide)

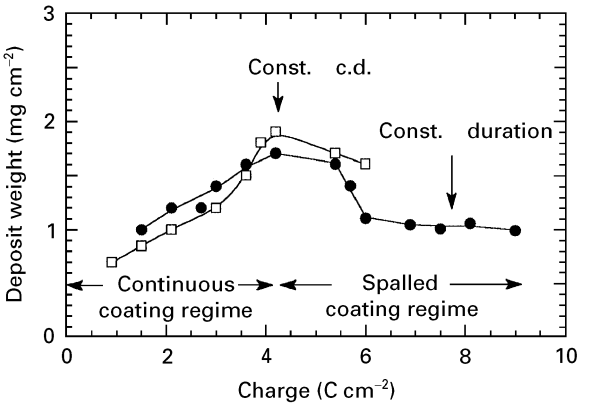

Figure 4 Deposit weight versus charge transferred to the cathode. The data in the continuous coating regime represent the master curve for electrodeposition on TiC substrates in a chromium-rich solution. $x = 0.1$.

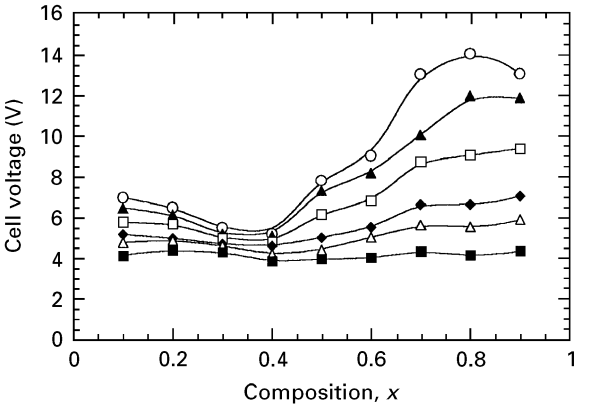

Figure 5 Cell voltage versus electrolyte composition at constant deposition durations of (■) 2, (△) 5, (◆) 7, (□), 10, (▲) 13 and (○) 15 min for TiC substrates at 5 mA cm^{-2}.

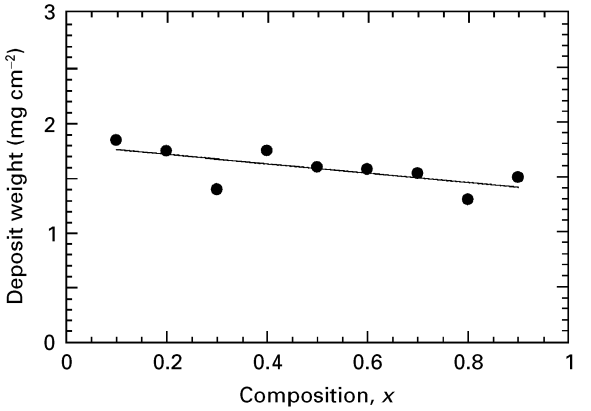

Figure 6 Deposit weight on TiC substrate versus electrolyte composition at constant deposition duration of 15 min and current density of 5 mA cm^{-2}.

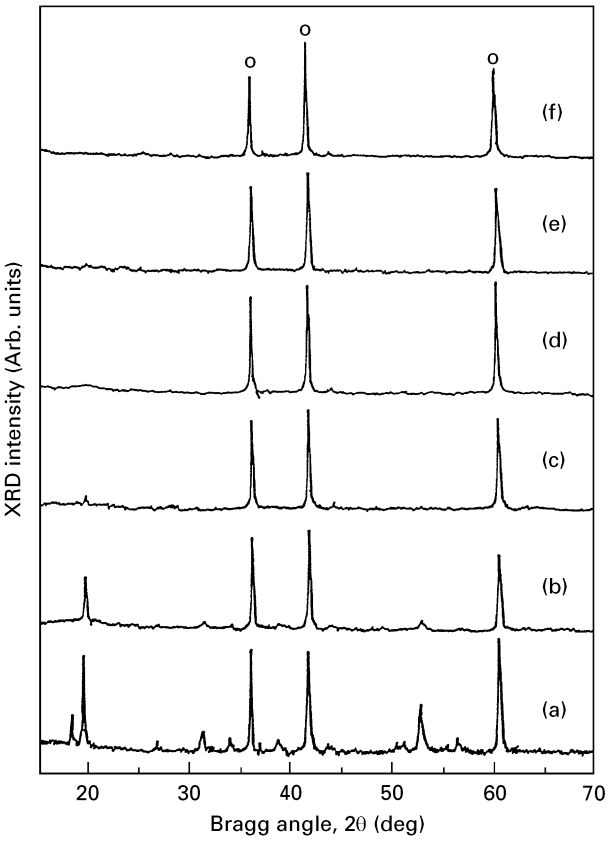

Figure 7 X-ray diffraction spectra of as-deposited coatings on TiC substrate, obtained from different electrolyte compositions: (a) $x = 0.1$; (b) $x = 0.2$; (c) $x = 0.3$; (d) $x = 0.4$; (e) $x = 0.5$; (f) $x = 0.9$; (o) substrate peaks.

[13, 14] or crystalline character (chromium oxide) [15].

The deposition parameters had a profound effect on coating morphology. As was pointed out above, low current density ($5\,mA\,cm^{-2}$) as well as deposition duration (15 min) have been selected in order to prevent spallation of the deposit (which is caused by the gas evolution and low adhesion). Fig. 8 shows the morphology of the as-dried coatings with different compositions. In all deposits, microcracks were observed after drying, which can be attributed to the drying shrinkage. The microcracks resulted in cracked-mud morphology of the deposits. (Preliminary supercritical drying experiments using the acetone/CO_2 system, resulted in reduction of the microcracking extent, but did not prevent it totally).

Table I summarizes the EDS chemical composition results of the as-dried coatings together with composition of the corresponding solutions, from which they were electrodeposited. In the coatings deposited from aluminium-rich solutions ($x = 0.9$), the aluminium and chromium contents were nearly similar to those in the starting solutions. For the equiatomic solutions ($x = 0.5$), the chromium content in the deposit was higher by a few per cent than the aluminium content. It can be concluded that deposition rate for the chromium component is higher than that of the aluminium component. It is believed that, for this reason, aluminium was not detected in the coatings deposited from chromium-rich solutions ($x = 0.1$).

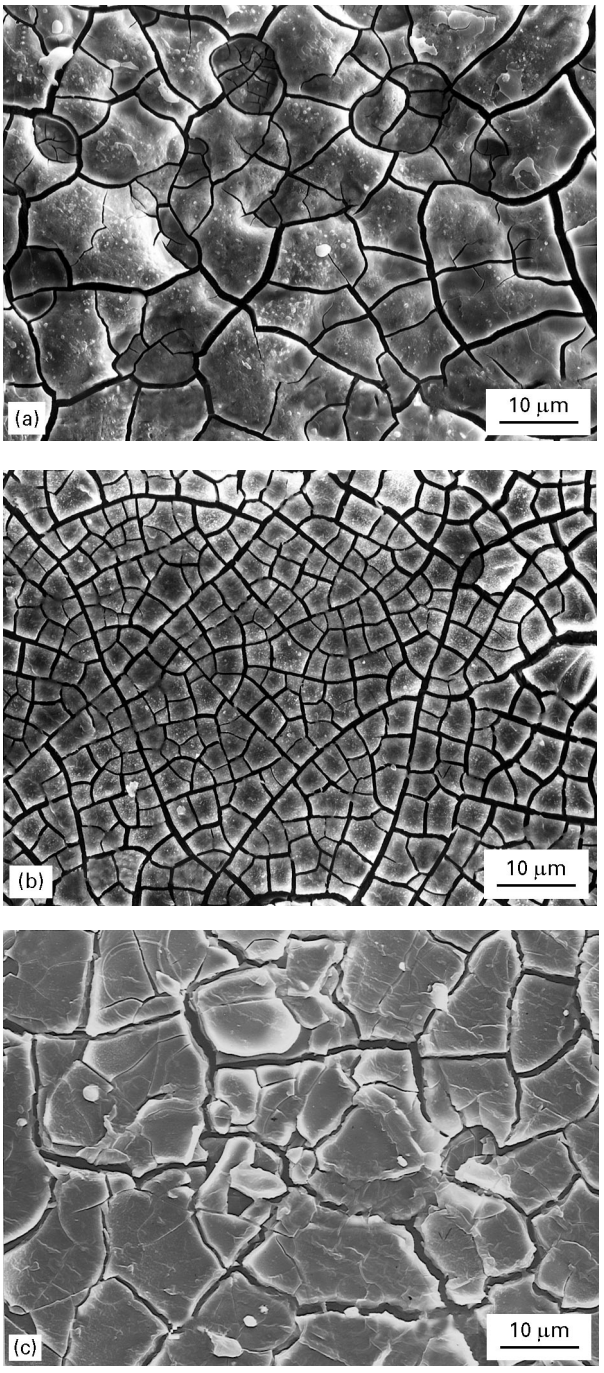

Figure 8 SEM images of green deposits on TiC substrates for c.d. $= 5\,mA\,cm^{-2}$ and deposition duration of 15 min using different electrolyte compositions: (a) $x = 0.1$; (b) $x = 0.5$ and (c) $x = 0.9$.

TABLE I Comparative results of the aluminium and chromium contents[a] in the solutions and in their corresponding deposits

Solution (at %)		Deposit (at %)	
Al	Cr	Al	Cr
90	10	88.6–90.7	9.3–11.4
50	50	43.4–47.5	52.5–56.6
10	90	0	100.0

[a]Al + Cr = 100%.

The compositional homogeneity of the as-deposited coatings was investigated by elemental mapping with EDS with appropriate statistical treatment (digimap). These analyses were performed on green coating

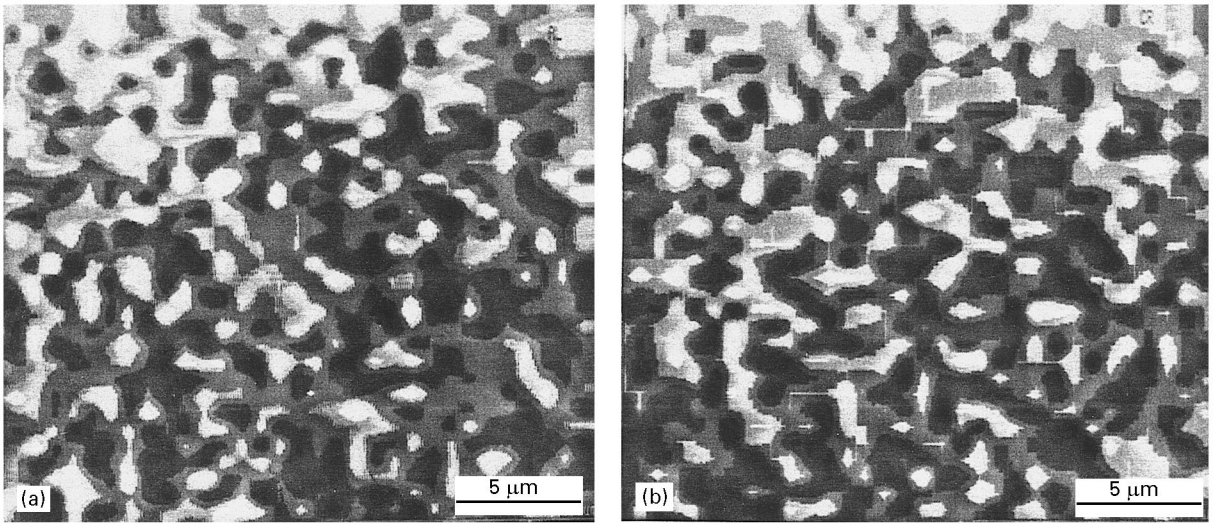

Figure 9 EDS digimaps of (a) aluminium and (b) chromium as the coating elements, and (c) titanium as the substrate element.

islands of about 30 μm diameter; the point step corresponded to the spatial resolution of the technique (probe size) of about 0.76 μm, with 200 ms acquisition time per point. The digitized mapping of aluminium and chromium as the coating elements and titanium as a substrate element are shown in Fig. 9. These digimaps indicated a uniform composition within the alumina–chromia deposits in the micrometre size range. In order to study the effect of coating thickness on the digimap patterns, the latter were subjected to EDS point analyses at different locations on the deposit. Similar results were found for five different analysis points with a standard deviation of ± 1.42 (2% accuracy) which is a typical s.d. for EDS results of homogeneous materials.

3.2. Electrodeposition on TiB_2 substrates

Electrodeposition experiments on TiB_2 substrates were performed at a c.d. of 5 mA cm^{-2} and deposition durations up to 16 min. The experimental results were very similar to those obtained for TiC substrates. Deposit weight was found to increase with deposition duration to a saturation value; a typical dependence is shown in Fig. 10. The change in cell voltages was found again to be composition dependent. Examination of composition dependencies on voltage at different stages of the electrodeposition revealed the presence of a minimum near the composition of $x = 0.3$–0.4 (Fig. 11). The deposit weight was also studied as a function of electrolyte composition at a fixed c.d. of 5 mA cm^{-2} and deposition duration of 15 min. These results, which are shown in Fig. 12, indicate a decrease in deposit weight with increase in aluminium content of the electrolyte. It is noteworthy that these deposit weights are very close to those obtained by electrodeposition on TiC substrates at the same experimental conditions. XRD spectra of the green deposits having different compositions are shown in Fig. 13. Well-defined crystalline peaks were recorded from deposits with compositions of $x = 0.1$ and 0.2, in addition to the peaks from the TiB_2 substrate (peaks marked "○"). No evidence for crystalline phases was found in the XRD spectra of the deposits prepared from solutions with $x > 0.3$. These crystallographic findings are in agreement with those found for the coatings deposited on to TiC substrates. The morphology of the coatings on TiB_2 substrates was also similar to that observed on the TiC substrates.

3.3. Electrodeposition on SiC substrates

Electrodeposition experiments were conducted in order to find the proper deposition conditions for the SiC substrates, because these substrates have a higher electrical resistivity relative to that of TiC and TiB_2. Based on these experiments, a c.d. of 10 mA cm^{-2} and deposition durations up to 5 min were found to yield continuous deposits without spallation. Fig. 14 shows a typical dependence of deposit weight on deposition duration. Deposit weight increased to a maximum above which spallation occurred. The net deposit weight was higher than that obtained on TiC and TiB_2 substrates, indicating that thicker coatings may form on SiC substrates. Again, deposit weight decreased linearly with increase in aluminium content, x, of the electrolyte (Fig. 15) similar to the trends found

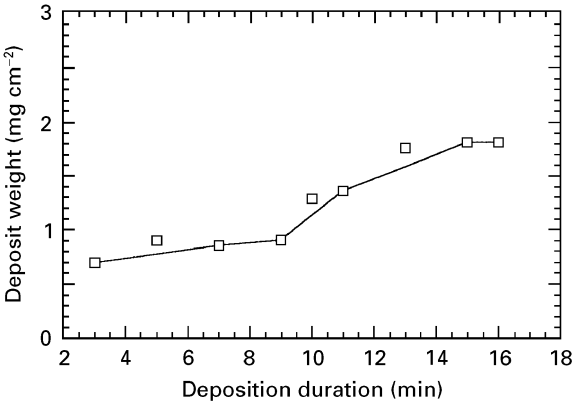

Figure 10 Deposit weight versus deposition duration for TiB_2 substrates at 5 mA cm^{-2} and $x = 0.1$.

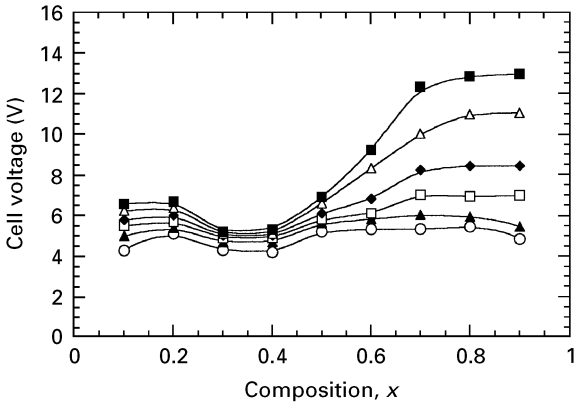

Figure 11 Cell voltage versus electrolyte composition at constant deposition durations of (○) 2, (▲) 5, (□) 8, (◆) 10, (△) 13, (■) 15 min for TiB_2 substrates, at 5 mA cm^{-2}.

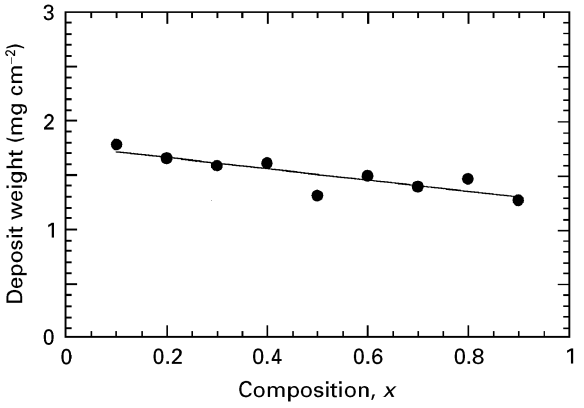

Figure 12 Deposit weight on TiB_2 substrates versus electrolyte composition at 5 mA cm^{-2} and 15 min.

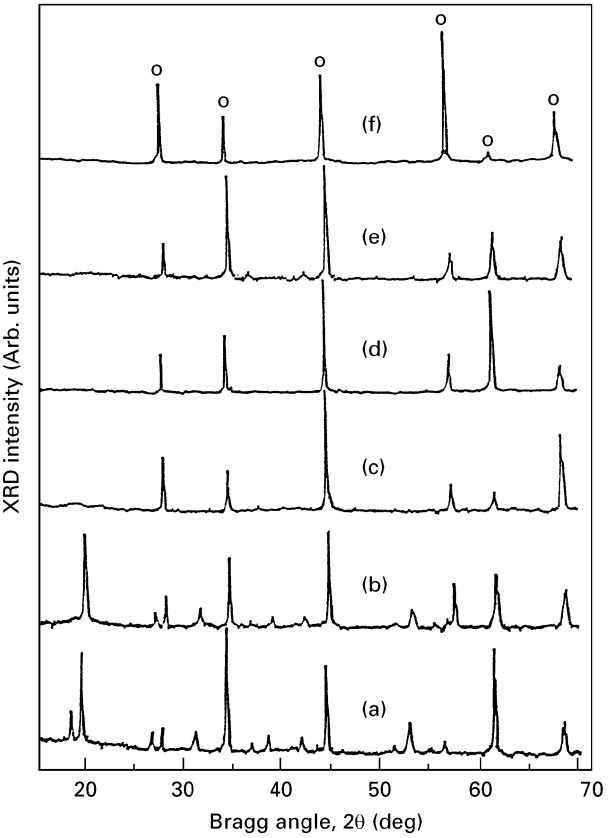

Figure 13 X-ray diffraction spectra of as-deposited coatings on TiB_2 substrates, obtained from different electrolyte compositions: (a) $x = 0.1$; (b) $x = 0.2$; (c) $x = 0.3$; (d) $x = 0.4$; (e) $x = 0.5$; (f) $x = 0.9$; (o) substrate peaks.

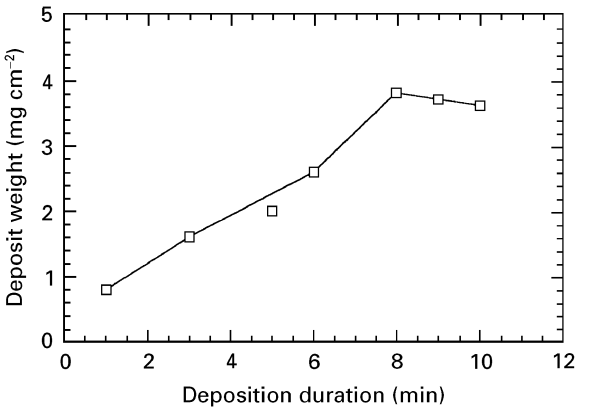

Figure 14 Deposit weight versus deposition duration for SiC substrates at 10 mA cm^{-2} and $x = 0.1$.

for TiC and TiB_2 substrates. As expected, the increase in cell voltage differed for different electrolyte compositions. Cell voltage versus electrolyte composition is shown in Fig. 16 and the dependencies resemble that observed for TiC and TiB_2 substrates (Figs 5 and 11, respectively) with the ubiquitous minimum at a composition of about $x = 0.3$. However, another two minima may also be observed at $x = 0.6$ and $x = 0.8$; the latter disappeared during stages of the deposition. However, owing to the lack of resolution in the composition axis, the existence of the latter maximum is uncertain. The X-ray diffraction spectrum (not shown here) revealed the green coatings with compositions $x \leqslant 0.3$ to be crystalline. These points will be further discussed below.

4. Discussion

The formation mechanism of ceramic coatings via the cathodic process was described in recent publications

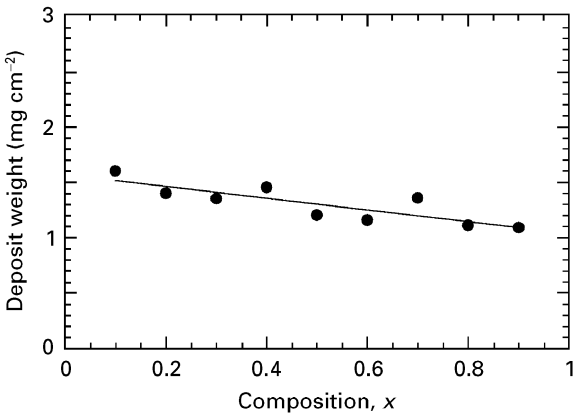

Figure 15 Deposit weight versus electrolyte composition using SiC substrates, at 10 mA cm^{-2} and 5 min.

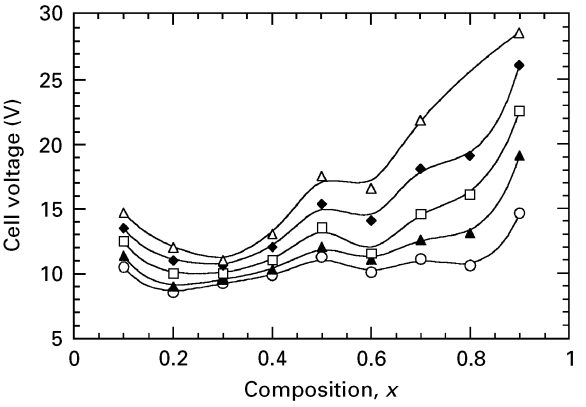

Figure 16 Cell voltage versus electrolyte composition at constant deposition durations of (○) 1, (▲) 2, (□) 3, (◆) 4 and (△) 5 for SiC substrates, at 10 mA cm^{-2}.

[14, 15, 19, 20] and the corresponding chemical reactions which underly the deposition process were discussed. The deposit build-up is based on dissociation of the metal nitrate and its hydrolysis via hydroxyl generated at the cathodic substrate. Hydrolysis of the metal cations is expected to form metal–oxygen polyanions, the composition of which depends on the pH of the solution as well as the electronegativities of the aqueous solution and the hydrolysed precursor. Further migration of these polyanions to the cathode surface is facilitated by electrophoresis. At this stage, deposition of the polyanions is basically governed by the wettability and electrical conductivity of the cathodic substrate. However, once a continuous layer is formed on the cathode, its further growth depends on the deposit properties (conductivity, density, thickness) rather than the substrate properties. In this respect, if the salt anions have a strong complexing ability, they may be incorporated within the structure or be adsorbed on the surface of the polyanion species. This will cause random arrangement of the latter at the growing deposit surface, and thus lead to an amorphous deposit. Nevertheless, anions with poor complexing ability may not be incorporated in the structure but only be adsorbed on the polyanion surfaces, and be released during the rearrangement of those polyanions that reach the cathodic surfaces. In such a case, crystalline hydroxide or water-adsorbed oxide deposits may result. With respect to our recent results [13–15] and the present findings, it seems that the nitrate ions have strong complexing ability with aluminium cations but a weak complexing ability with the chromium cations. Therefore, while chromium-rich deposits were found to be crystalline, aluminium-rich deposits were amorphous.

For experiments performed in the galvanostatic regime, the cell voltage is an important characteristic of the deposition process. As a first approximation, at constant current, i, the cell voltage, V, can be expressed as

$$V = V_0 + iR_s + iR_d \quad (1)$$

where V_0 is constant for a given solution and electrode, R_s and R_d are the resistances of the solution and the deposit, respectively. Chromium and aluminium oxides differ in their electrical resistivities by several orders of magnitude (10^7 and $10^{14}\,\Omega$ cm, respectively). Although the resistivities of their corresponding oxyhydroxides (the actual deposit compositions) are not known, they are expected still to be far higher than those of the cathode substrates. During the deposition process, R_d increases with the deposit thickness, resulting in an increase of the voltage drop, iR_d, across the deposit. Thus, cell voltage will increase with time during deposition (Figs 1, 5, 11 and 16) and its behaviour is influenced by the deposition rate, which in turn is expected to increase with current density (Fig. 1). The cell voltage is also sensitive to defects within the coating which may appear at high deposit thicknesses owing to local breakdown or deposit spallation [2, 14].

Adhesion of the deposit to the substrate is one of the major factors controlling the maximum mass to be deposited. The maximum deposit weight may be estimated from the master curve (Fig. 4). Substrates with high electrical conductivity and which are inert to hydrogen bonds (such as platinum) will exhibit poor adhesion of the deposit, and will lead to sedimentation of a powdery precipitate. Increase in the covalency of the substrate material from $TiB_2 \rightarrow TiC \rightarrow SiC$ is expected to enhance their tendency to form hydrogen bonds with the deposit. This postulation is in agreement with the higher deposit weights formed at similar electrochemical conditions on SiC relative to those formed on TiB_2 and TiC substrates.

Other factors that control the deposit weight are electrical conductivity of the deposit and current density. The higher the electrical conductivity of the deposit, the higher is its tendency for electrocrystallization during the electrodeposition and thicker deposits can be formed. The lower is the current density, the lower is the deposition rate, and denser deposits will be formed. These expectations are in agreement with Switzers' work [1] on electrochemical synthesis of ceric oxide powders as well as with our recent works [13–15].

Another inherent problem in the deposition process is the gas evolution, which also initiates formation of defects within the deposit. Deposit spallation and local breakdown result in local decrease of the deposit

electrical resistance. This in turn will induce high local current densities which facilitate water hydrolysis and evolution of molecular hydrogen at the cathode surfaces. As a result, the cell voltage decreases, and so does the corresponding maximum of the voltage–deposition duration curve (Fig. 1) that may be related to this process. At deposition durations beyond the maximum, deposit continues to form, but the deposition rate in the undamaged areas is significantly lower. In contrast, c.d.s and deposition rates are much higher in defected regions. This effect is expected to speed up the restoration of the spalled regions. However, with lapse of time, when the surface density of the defected regions increases, the deposit thickness becomes non-uniform.

As a possible explanation of the minima observed in the voltage–electrolyte composition curves (Figs 5, 11 and 16) we will consider the change in the electrical resistance of the deposit due to the composition and the degree of crystallinity. No appreciable variations in the conductivity of the starting solution were observed with composition. Moreover, the minima became more pronounced with increase in coating thickness. In addition, no shifting of the minima was observed with composition. A possible link emerges between the minima in the voltage–composition curves and the X-ray data. X-ray results showed that the as-deposited coatings were amorphous for compositions with $x \geqslant 0.3$, or include an amorphous phase together with a crystalline phase for $x < 0.3$. Because digimap results showed a homogeneous composition throughout the deposits, the latter could be considered as homogeneous mixtures of aluminium and chromium oxy-hydroxides. (These mixtures may act as precursor for the oxide solid solutions.) This is in accordance with the complete and mutual solid solubility of the chromium and aluminium oxides [21]. Moreover, it is well documented that the electrical resistivity of these solid-solution oxides may be varied with composition of the binary solid solutions [16]. Assuming a similar behaviour in the electrical conductivity of the mixed oxy-hydroxides, the increase in the chromium content of the deposit is believed to increase its electrical conductivity (most probably of ionic character). Therefore, the cell voltage decreases with increase in the chromium content. However, above a certain deposit composition ($x \approx 0.3$–0.4) crystallization of either the solid solution or the chromium-containing component of the deposit should decrease its ionic conductivity. Therefore, the cell voltage will increase again with composition towards the chromium-rich side of the composition range. In addition, Ristic *et al.* [22] reported on the presence of a crystalline phase in addition to the solid-solution phase, at the chromium-rich side of the alumina–chromia system.

It is important to note that the deposits obtained from a pure chromium nitrate solution showed a crystalline structure of the chromium hydroxide. This is in contrast to the results of Indira and Kamath [23] according to which cathodic deposits obtained from chromium nitrate solutions were found to be X-ray amorphous. They also reported the formation of crystalline aluminium hydroxide (bayerite) in contrast to our findings. These differences can be attributed to different experimental conditions such as the electrolyte concentration (0.3 M versus 0.1 M), temperature (25 versus 10 °C) and current density (65 versus 5 mA cm^{-2}). In this regard, recent results on electrodeposition from lead nitrate [20] have shown that deposits with different compositions can be obtained by varying the electrolyte concentration. From codeposition experiments in the alumina–chromia system performed in the present work it has been concluded that certain regions of crystallinity exist for the deposit (with $x < 0.3$). Indira *et al.* [24] found that in the nickel-based binary systems with aluminium, chromium, manganese and iron, the amorphicity of one component imposed amorphicity to the complex hydroxide. Our findings indicate that this rule does not hold for the alumina–chromia system.

Another point to refer to is the deposit morphology. In the present work, short deposition durations were applied in order to prevent deposit spallation and to optimize the deposit morphology (thickness homogeneity, low surface roughness, etc.). However, microcracks were observed in the deposit after drying (Fig. 8), which can be attributed to the drying shrinkage. In order to protect the non-oxide ceramic substrate at elevated temperatures, it is important to prevent formation of microcracks and other defects within the coatings. Deposit microcracking associated with drying shrinkage is a common problem in the wet chemical methods, once thick coatings are formed. Results of supercritical drying experiments on sol–gel derived coatings [25] indicate that this method is ineffective in avoiding microcrack formation in relatively thick coatings. More promising are decreasing current density as well as increasing bath temperature [26] which lead to denser green coatings with a lower probability for microcracking.

Acknowledgements

This research was supported by a grant of the Israel Ministry of Science and the Arts and of Forschungszentrum Juelich GmbH (KFA) – Projecktträger fuer Biologie, Material und Rohstofforschung (PLR) Germany. Dr A. Berner is acknowleged for performing the digimap analyses.

References

1. J. A. SWITZER, *Am. Ceram. Soc. Bull.* **66** (1987) 1521.
2. L. GAL-OR, I. SILBERMAN and R. CHAIM, *J. Electrochem. Soc.* **138** (1991) 1939.
3. R. CHAIM, I. SILBERMAN and L. GAL-OR, *ibid.* **138** (1991) 1942.
4. K.-C. HO, *ibid.* **134** (1987) 52C.
5. S. B. ABOLMAALI and J. B. TALBOT, *ibid.* **140** (1993) 443.
6. P. BENDALE, S. VENIGALLA, J. R. AMBROSE, E. D. VERNIK Jr. and J. H. ADAIR, *J. Am. Ceram. Soc.* **76** (1993) 2619.
7. R. BACSA, P. RAVINDRANATHAN and J. P. DOUGHERTY, *J. Mater. Res.* **7** (1992) 423.
8. M. SHIRCHANZADEH, M. AZADEGAN, V. STAK and S. SCHREYER, *Mater. Lett.* **18** (1994) 211.

9. Y. MATSUMOTO, T. MORIKAWA, H. ADACHI and J. HOMBO, *Mater. Res. Bull.* **27** (1992) 1319.
10. Y. MATSUMOTO, H. ADACHI and J. HOMBO, *J. Am. Ceram. Soc.* **76** (1993) 769.
11. J. A. SWITZER, *Nanostruct. Mater.* **1** (1992) 43.
12. R. CHAIM, *ibid.* **1** (1992) 479.
13. R. CHAIM, G. STARK, L. GAL-OR and H. BESTGEN, *J. Mater. Sci. Lett.* **13** (1994) 487.
14. *Idem., J. Mater. Sci.* **29** (1994) 6241.
15. R. CHAIM, S. ALMALEH-ROCKMAN, L. GAL-OR and H. BESTGEN, *J. Am. Ceram. Soc.* **77** (1994) 3202.
16. E. ELSHEREEFY and M. F. R. FOUDA, *J. Mater. Sci. Lett.* **10** (1991) 299.
17. R. C. BRADT, *J. Am. Ceram. Soc.* **50** (1967) 54.
18. B. B. GHATE, W. C. SMITH, C. H. KIM, D. P. H. HASSELMAN and G. E. KANE, *Am. Ceram. Soc. Bull.* **54** (1975) 210.
19. I. ZHITOMIRSKY, L. GAL-OR and S. KLEIN, *J. Mater. Sci. Lett.* **14** (1995) 60.
20. I. ZHITOMIRSKY, L. GAL-OR, A. KOHN and H. W. HENNICKE, *ibid.* **14** (1995) 807.
21. E. M. LEVIN, C. R. ROBBINS and H. F. McMURDIE (eds.), "(American Phase Digramms for Ceramists", Ceramic Society, Columbus, OH, 1979) p. 121.
22. M. RISTIC, S. POPOVIC and S. MUSIC, *Mater. Lett.* **16** (1993) 309.
23. L. INDIRA and P. V. KAMATH, *J. Mater. Chem.* **4** (1994) 1487.
24. L. INDIRA, M. DIXIT and P. V. KAMATH, *J. Power Sources* **52** (1994) 93.
25. D. B. GUNDEL, P. J. TAYLOR and F. E. WAWNER, *J. Mater. Sci.* **92** (1994) 1795.
26. R. CHAIM, I. ZHITOMIRSKY, L. GAL-OR and H. BESTGEN, *J. Mater. Sci.* **32** (1997) 389.

Received 15 December 1995
and accepted 4 April 1996